Complete Physical Characterization of Quantum Nondemolition Measurements via Tomography

L. Pereira,* J. J. García-Ripoll, and T. Ramos†
Instituto de Física Fundamental IFF-CSIC, Calle Serrano 113b, Madrid 28006, Spain

(Received 29 September 2021; accepted 3 June 2022; published 29 June 2022)

We introduce a self-consistent tomography for arbitrary quantum nondemolition (QND) detectors. Based on this, we build a complete physical characterization of the detector, including the measurement processes and a quantification of the fidelity, ideality, and backaction of the measurement. This framework is a diagnostic tool for the dynamics of QND detectors, allowing us to identify errors, and to improve their calibration and design. We illustrate this on a realistic Jaynes-Cummings simulation of a superconducting qubit readout. We characterize nondispersive errors, quantify the backaction introduced by the readout cavity, and calibrate the optimal measurement point.

DOI: 10.1103/PhysRevLett.129.010402

Introduction.—Quantum nondemolition (QND) detectors measure an observable preserving its expectation value [1,2]. This property is essential in backaction-free quantum metrology [3–7], and in quantum protocols with feedback, e.g., fault tolerant computation [8–12]. QND measurements are typically implemented indirectly by monitoring a coupled subsystem, as demonstrated in various AMO [13–17] and solid-state [18–23] platforms. In superconducting circuits, the standard qubit measurement is a dispersive readout [24] mediated by frequency shifts in an off-resonant cavity. This is a near-QND process that approximately preserves the qubit's polarization [cf. Fig. 1(b)], and enables rapid high-fidelity single-shot measurements [25,26], protection by Purcell filters [27–30], fast reset [31], and simultaneous readout through frequency multiplexing [28,30,32].

State-of-the-art QND detectors still face experimental challenges. A critical problem is the exponential accumulation of backaction errors from repeated applications of the detector, which limits the scaling of quantum technologies. In a superconducting qubit readout, such errors originate in deviations from the dispersive limit in practical devices [33–35]. This has motivated more complex QND measurement schemes [36–44], which also introduce their own sources of imperfection.

In order to make progress in the design and operation of QND measurements, we need a complete and self-consistent diagnostic tool, which helps both with the calibration of the detector and with describing its real dynamics. Many experiments have focused on optimizing simple quantities such as the readout fidelity and the QND-ness [40,43]. However, these fidelities do not quantify the QND nature of a measurement, but rather its projectivity and ideality as shown below. Another standard approach is detector tomography [45–49]. This method characterizes destructive measurements via positive operator-valued measurements (POVMs), but ignores the postmeasurement state, and therefore a description of the measurement backaction.

In this Letter, we develop a complete physical characterization of QND measurements and their backaction via quantum tomography. The protocol, without precalibration of the QND detector, estimates both the POVM elements and the quantum process operators associated to each measurement outcome. As seen in Fig. 1(a), this requires

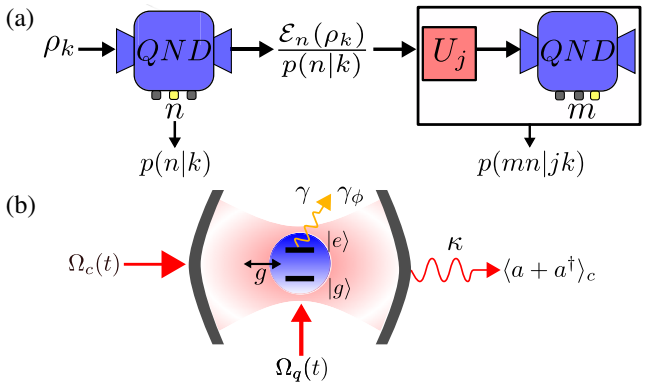

FIG. 1. (a) QND detector tomography for generic measurements. A self-consistent calibration requires sampling over input states ρ_k and two consecutive QND measurements, interleaved by a unitary operation U_j. This allows us to generate the measurement processes $\mathcal{E}_n$, for each possible outcome $n = 1, \ldots, N$, and to reconstruct them tomographically from the conditional probabilities $p(n|k)$ and $p(mn|jk)$. (b) Setup for tomographic characterization of QND qubit readout. It requires pulse control on qubit $\Omega_q(t)$ and cavity $\Omega_c(t)$, as well as continuous homodyne detection $\langle a + a^\dagger \rangle_c$. The detector can have arbitrary qubit-cavity coupling g and any imperfection such as qubit decay γ and dephasing γ_ϕ.

two consecutive applications of the detector, interleaved by unitary operations, and repeated over a set of input states. The information contained in the process operators can be used to identify errors, calibrate, and optimize the design of QND detectors. This can be done either directly, or through the analysis of simple metrics such as readout fidelity, QND-ness, and *destructiveness*, a precise bound of the measurement backaction that we introduce below. The method can be applied to any detector, but we illustrate its power simulating realistically the calibration of superconducting qubit readout beyond the dispersive approximation. Our study shows that state-of-the-art dispersive readout is a near-ideal measurement at the optimum of QND-ness, but there are other regimes where it becomes maximally QND with minimal backaction error, as revealed by the destructiveness. Other tomographic approaches to nondestructive detectors focus on near-ideal measurements only [50,51], and thus do not provide a characterization of their real QND nature.

General description of QND measurements.—A nondestructive quantum measurement with N outcomes is represented by N completely positive maps $\mathcal{E}_n$, which add up to a trace-preserving map $\mathcal{E} = \sum_n \mathcal{E}_n$. The nth measurement outcome is obtained with probability $p(n) = \mathrm{Tr}\{\mathcal{E}_n(\rho)\}$, leaving the system in the postmeasurement state $\rho_n = \mathcal{E}_n(\rho)/p(n)$. Each $\mathcal{E}_n$ is unambiguously represented by the Choi matrix Υ_n, whose d^4 elements Υ_n^{ijkl} read as

$$\Upsilon_n^{ijkl} = \langle ij|\Upsilon_n|kl\rangle = \langle i|\mathcal{E}_n(|k\rangle\langle l|)|j\rangle, \tag{1}$$

with $\{|i\rangle\}$ a basis of the measured system with dimension d. The Choi matrices give the postmeasurement states $\mathcal{E}_n(\rho) = \sum_{ijkl} \Upsilon_n^{ijkl}\rho^{kl}|i\rangle\langle j|$ [52] and also the measurement statistics $p(n) = \mathrm{Tr}\{\Pi_n\rho\}$, with the POVM elements, $\Pi_n = \sum_{ijk} \Upsilon_n^{kjki}|i\rangle\langle j|$. Conservation of probability requires the completeness relation, $\sum_n \Pi_n = \mathbb{1}$, which imposes $\sum_{nk} \Upsilon_n^{kjki} = \delta_{ij}$ on the Choi components.

A QND measurement of observable O [2,54,55] is one where the unconditional process $\mathcal{E} = \sum_n \mathcal{E}_n$ conserves the probability distribution $p(n)$ over repeated measurements. Equivalently, $\mathcal{E}$ preserves the average of all compatible observables O_c

$$\langle O_c\rangle = \mathrm{Tr}\{O_c\rho\} = \mathrm{Tr}\{O_c\mathcal{E}(\rho)\}, \quad \forall\ [O_c, O] = 0. \tag{2}$$

Ideal measurements are well known QND measurements where consecutive detections project the system onto the same eigenstate of O. This requires all Choi matrices to be projectors $\Upsilon_n = (\Upsilon_n)^2$, a sufficient condition to satisfy Eq. (2). However, as shown below, general QND measurements are not ideal, and allow the state of consecutive detections to change, provided the averages $\langle O_c\rangle$ remain constant.

Tomographic reconstruction of measurement processes.—We have developed a self-consistent characterization of QND measurements, based on two consecutive applications of the detector, interleaved with unitary operations from a universal set of gates U_j [cf. Fig. 1(a)]. The first measurement induces the processes $\mathcal{E}_n$, conditioned on the detected outcome, while the unitary U_j and the second measurement are used for a process tomography of the detector itself. By repeating the protocol over a set of input states ρ_k, we obtain the conditional probabilities $p(n|k) = \mathrm{Tr}(\Pi_n\rho_k)$ and $p(mn|jk) = \mathrm{Tr}[\Pi_m U_j\mathcal{E}_n(\rho_k)U_j^\dagger]$ after the first and second measurements, respectively. From these distributions we reconstruct the POVMs Π_n and Choi matrices Υ_n that best approximate the measurement, without a precalibration of the detector.

To recover matrices Π_n and Υ_n that are meaningful and satisfy all the physical constraints of a measurement, we use maximum likelihood estimation [48,56,57] in a two-step strategy. First, we reconstruct the POVMs by minimizing the log-likelihood function $f(\{\Pi_j\}) = \sum_{n,k} \hat{p}(n|k)\log[\mathrm{Tr}(\Pi_n\rho_k)]$, which compares the experimental probabilities $\hat{p}(n|k)$ to the set of feasible matrices $\{\Pi_n\}$ satisfying $\Pi_n \geq 0$ and $\sum_n \Pi_n = \mathbb{1}$. Finally, we estimate the Choi matrices Υ_n, minimizing a function $f_n(\Upsilon_n) = \sum_{mjk} \hat{p}(mn|jk)\log\mathrm{Tr}[(U_j^\dagger\Pi_m U_j \otimes \rho_k^T)\tilde{\Upsilon}_n]$ which compares the experimental probabilities $\hat{p}(mn|jk)$ to a parametrization of the Choi matrix Υ_n satisfying $\tilde{\Upsilon}_n \geq 0$ ($\tilde{\Upsilon}_n^{ijkl} = \Upsilon_n^{ikjl}$) and the POVM constraint $\Pi_n = \sum_{ijk} \Upsilon_n^{kjki}|i\rangle\langle j|$. In total, QND detector tomography solves $N+1$ optimization problems: one for POVMs of size d^2, and N for Chois of size d^4 [58].

QND measurement quantifiers via tomography.—We use the reconstructed Choi matrices Υ_n to quantify the performance and QND nature of a measurement. Standard benchmarks for QND detectors are readout fidelity $F = \sum_n p(n|n)/N$ and QND-ness $Q = \sum_n p(nn|n)/N$, defined as the average probability that an observable's eigenstate $|n\rangle$ remains unchanged after one or two measurements, respectively. These quantities are related to tomography via

$$F = \frac{1}{N}\sum_n \langle n|\Pi_n|n\rangle = \frac{1}{N}\sum_{nj} \Upsilon_n^{njnj}, \tag{3}$$

$$Q = \frac{1}{N}\sum_n \langle nn|\Upsilon_n|nn\rangle = \frac{1}{N}\sum_n \Upsilon_n^{nnnn}. \tag{4}$$

The readout fidelity F quantifies how close the measurement is to a *projective* one $\Pi_n = (\Pi_n)^2$. QND-ness Q and other similar fidelities [51] quantify the overlap with an *ideal measurement*, satisfying $\Upsilon_n = (\Upsilon_n)^2$. Both are important measurement properties, but none of them assess the QND nature of the detector and its backaction on the

observables [Eq. (2)]. For instance, a maximum value $Q = 1$ characterizes an ideal measurement, but there are nonideal measurements $Q \neq 1$ which are close to QND. Nonideal QND measurements are useful in quantum tasks that only require evaluating observable averages such as variational algorithms or sensing [59–64].

We introduce the *destructiveness* D as a precise quantifier of the QND nature of a detector, regardless of how ideal it is. This new quantifier bounds the change or backaction suffered by any observable compatible with the measurement of O, in accordance with property (2):

$$D = \frac{1}{2} \max_{\|O_c\|=1} \|O_c - \mathcal{E}^\dagger(O_c)\|, \qquad [O, O_c] = 0. \quad (5)$$

Evaluating D requires the tomographic reconstruction of the complete measurement process, $\mathcal{E}^\dagger(O_c) = \sum_{ijkln} [\Upsilon_n^{klij}]^* O_c^{kl} |i\rangle\langle j|$, and a maximization over all compatible operators of unit norm $\|O_c\| = 1$, with $\|O\| = \sqrt{\mathrm{Tr}(O^\dagger O)}$. In practice, this maximization is done by finding the maximum eigenvalue of a positive matrix [59]. For instance, in the case of the qubit observable $O = \sigma_z$, the destructiveness reduces to $D = \|\sigma_z - \mathcal{E}^\dagger(\sigma_z)\|/\sqrt{8}$. Since D verifies the general QND condition [Eq. (2)], it also bounds the change of the probability distribution $p(n)$ over repeated measurements.

As shown below, the three quantities F, Q, and D describe the most important aspects of QND detectors, but there is further information to extract from Υ_n, which are the most general objects.

Calibration of qubit readout beyond dispersive approximation.—In a standard superconducting qubit readout [24], the qubit $\{|g\rangle, |e\rangle\}$ couples to an off-resonant cavity mode a with detuning Δ and coupling g [cf. Fig. 1(b)]. For a highly anharmonic qubit, such as the flux qubit, this interaction is described by a Jaynes-Cummings (JC) Hamiltonian [65],

$$H_{\mathrm{JC}} = \frac{\Delta}{2}\sigma_z + g(\sigma_+ a + a^\dagger \sigma_-) + \Omega_c(t)(a + a^\dagger), \quad (6)$$

with Pauli operators $\sigma_z = |e\rangle\langle e| - |g\rangle\langle g|$, $\sigma_- = \sigma_+^\dagger = |g\rangle\langle e|$, and a resonant drive $\Omega_c(t)$ on the cavity. In the dispersive limit $\Delta \gg g$, H_{JC} approximates a dispersive model $H_d = \frac{1}{2}(\Delta + \chi)\sigma_z + \chi\sigma_z a^\dagger a + \Omega_c(t)(a + a^\dagger)$ that predicts a qubit-dependent displacement $\chi = g^2/\Delta$ on the cavity resonance. In theory, by continuous homodyne detection $\langle a + a^\dagger\rangle_c$ on the cavity, we can discriminate the qubit state without destroying it. In practice, the nondispersive corrections implicit in H_{JC} can slightly degrade the QND nature of the measurement [33,66].

To realistically quantify the performance and measurement backaction of the dispersive readout, we describe the dynamics with the full H_{JC} and a stochastic master equation

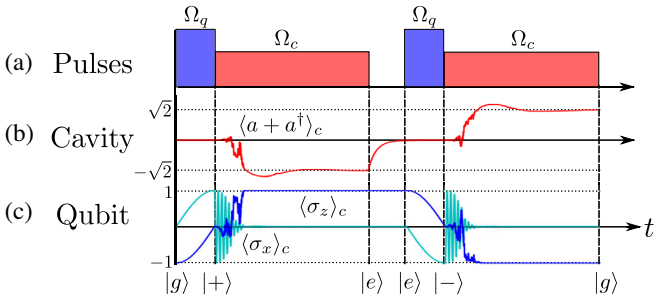

FIG. 2. Simulation of QND detector tomography for dispersive qubit readout. (a) Pulse scheme on qubit (blue) and cavity (red) to implement state preparation, gates, and homodyne measurements. (b) Cavity quadrature $\langle a + a^\dagger\rangle_c$ conditioned on a single trajectory. (c) Average of Pauli operators $\langle\sigma_z\rangle_c$ (blue) and $\langle\sigma_x\rangle_c$ (light blue) conditioned on the same trajectory. This realization corresponds to an initial state $|+\rangle = (|g\rangle + |e\rangle)/\sqrt{2}$ on the qubit, a first measurement with outcome $|e\rangle$, a cavity reset time, the use of gate $\exp(-i\pi\sigma_y/2)$, and a second measurement with outcome $|g\rangle$. Repeating this procedure over many trajectories with different inputs and gates allows us to reconstruct the Choi matrices Υ_g and Υ_e.

(SME) [67–70]. This formalism accounts for the backaction of the continuous homodyne detection onto the qubit state, as well as cavity decay κ, qubit decay γ, and qubit dephasing γ_ϕ [59]. We simulate numerically the tomographic procedure, solving the SME over many realizations of the experiment [71]. On each trajectory, the qubit is prepared in one of the six states $\rho_k \in \{|g\rangle, |e\rangle, (|g\rangle \pm |e\rangle)/\sqrt{2}, (|g\rangle \pm i|e\rangle)/\sqrt{2}\}$. We perform two single-shot measurements, interleaved by a cavity reset time, and one of the three qubit gates $U_j \in \{\mathbb{1}, \exp(-i\pi\sigma_y/4), \exp(-i\pi\sigma_x/4)\}$. In Fig. 2 we show a representative trajectory of the protocol, where the outcome of each single-shot measurement is discriminated as $\langle\sigma_z\rangle_c = -\mathrm{sign}(J)$ with $J = \sqrt{\kappa}\int_0^T dt\langle a + a^\dagger\rangle_c$ the homodyne current integrated over the duration T of the readout pulse $\Omega_c(t)$ [59]. For simplicity of the simulation, we neglect imperfections in the qubit state preparation and gates, performed with a local control $\Omega_q(t)$. In a real experiment, these imperfections can be self-consistently separated from intrinsic measurement errors by using standard gate set tomography [72–74]. Simulations consider state-of-the-art parameters of superconducting qubit readout [26,75,76]: $g/2\pi = 200$ MHz, $\kappa = 0.2\ g$, $\gamma = \gamma_\phi = 10^{-4} g$, $T = 8/\kappa \approx$ 32 ns, and $|\Omega_c| = 0.173\ g$, corresponding to $\langle a^\dagger a\rangle \sim 1.5$ photons on cavity for $2\chi/\kappa = 1$.

We calibrate the measurement by tuning Δ/g and computing via tomography the quantifiers $1 - F$, $1 - Q$, and D [cf. Fig. 3(a)]. We show predictions using the realistic H_{JC} interaction (solid), as well as the dispersive model H_d (dashed) to benchmark the results. We identify three qualitatively different points of operation, (i)–(iii), as indicated by vertical lines in Fig. 3(a). For each of them, we

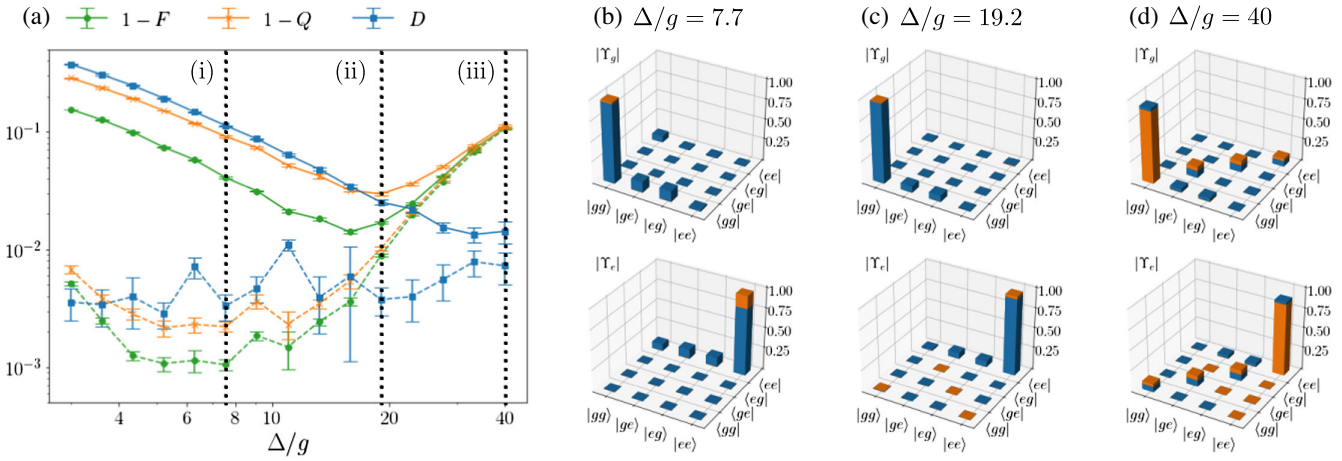

FIG. 3. Measurement quantifiers and reconstructed Choi matrices for QND qubit readout. (a) Readout infidelity $1-F$ (green circles), QND-ness infidelity $1-Q$ (orange crosses), and destructiveness D (blue squares) as a function of Δ/g. Solid (dashed) lines correspond to predictions for JC (dispersive) models. (b)–(d) Choi matrices $|\Upsilon_n|$ for $n=e,g$ measurement outcomes at the three representative values $\Delta/g=[7.7, 19.2, 40]$, indicated by vertical lines in (a). Blue (orange) bars correspond to predictions from JC (dispersive) models. On each column, the upper color corresponds to the part of the longest bar that does not overlap with the shortest one (and thus a single color indicates full overlap). The probabilities to reconstruct Υ_n are estimated from 2×10^4 trajectories for each initial state ρ_k and gate U_j. Error bars correspond to 1 standard deviation, obtained from 10^3 bootstrap simulations. Parameters are indicated in text.

display in Figs. 3(b)–3(d) the Choi matrices $|\Upsilon_n|$ for both measurement outcomes $n=e,\ g$, where blue (orange) columns correspond to the JC (dispersive) predictions and the upper color corresponds to the higher values.

(i) Around $\Delta/g=7.7$, the dispersive model reaches its optimum in fidelity and QND-ness, and the measurement is nearly ideal with projective Choi matrices $\Upsilon_n^{(d)}\approx|nn\rangle\langle nn|$ [cf. orange columns in Fig. 3(d)]. This occurs near $2\chi/\kappa\sim1$ as expected by theory [24]. In contrast, the Choi matrices of the JC model show strong deviations from an ideal measurement [cf. blue columns in Fig. 3(b)]. The population transfer $|e\rangle\to|g\rangle$ during measurement—mainly due to cavity-induced Purcell decay [33]—reduces Υ_e^{eeee} and increases Υ_n^{ggee}. In addition, the increase of Υ_n^{genn} and Υ_n^{egnn} corresponds to the growth of qubit coherences during measurement—e.g., due to cavity-mediated qubit driving [66]. These nondispersive effects increase the infidelity and destructiveness [cf. Fig. 3(a)] and shift the optimal working point to larger Δ/g.

(ii) Around $\Delta/g=19.2$, the nondispersive corrections decrease, and the QND-ness reaches an optimum $Q\approx0.97$ where the actual measurement is most ideal. From Υ_n in Fig. 3(c), we observe that nondispersive effects are present but strongly suppressed. In contrast to the dispersive model, this optimum of QND-ness does not coincide with the optimum of fidelity [cf. Fig. 3(a)]. This is explained by noting that QND-ness is influenced by backaction D, while fidelity has no information about postmeasurement states and cannot depend on it. In the JC model, D decreases monotonically with Δ/g, and thus the condition of highest Q shifts toward larger Δ/g in order to minimize backaction [77]. In contrast, the backaction D of the dispersive model is nearly constant with Δ/g, and the optima of Q and F coincide.

(iii) Around $\Delta/g=40$ the system is deep in the dispersive limit. The predictions for both models almost coincide, up to residual cavity-mediated qubit driving [66]. Here, $1-F$ and $1-Q$ get worse, but D reaches its minimum, meaning that the realistic measurement is maximally QND, but less ideal than in (ii). The loss of ideality is clearly manifested by the large diagonal terms Υ_n^{mmll} [cf. Fig. 3(d)]. This behavior is explained theoretically in the Supplemental Material [59] by the low distinguishability between outcomes $n=g,e$ when the cavity displacement $\sim g^2/\Delta$ is too small compared with the measurement uncertainty $\sim\kappa$. The minimum value of D is attributed to how decoherence $\gamma=\gamma_\phi=10^{-4}\ g$ breaks the QND condition [Eq. (2)] even when nondispersive effects are suppressed, as shown in the Supplemental Material [59].

We see that a tomography-based calibration allows us to characterize different regimes of the detector, and to identify error sources via the process matrices Υ_n. When simulating the measurement dynamics with $H_{\rm JC}$, we account for all nondispersive effects and the backaction appearing in realistic superconducting circuit experiments, in a unified way. We also consider imperfections due to larger intrinsic qubit decay and dephasing on the operation points (ii) and (iii). The effect of intrinsic decay γ is qualitatively similar to Purcell decay, whereas pure dephasing γ_ϕ has a negligible effect on the Choi matrices for long readout pulses $T\gg1/\kappa$ [59]. Finally, our physical analysis can be used to choose an optimal working point for the detector. If one is interested in a near-ideal QND measurement, optimizing Q gives a good compromise between fidelity F and backaction D, as illustrated in (ii). This

requires a larger detuning Δ/g than expected by the standard dispersive prediction [24]. However, if one is interested in a maximally QND measurement with minimal backaction, D is a more suitable quantity to optimize. This may require losing ideality of the measurement as shown in (iii).

Conclusions and outlook.—We developed a tomographic procedure to calibrate and characterize arbitrary QND detectors via a reconstruction of the measurement processes Υ_n. We applied the method to a realistic simulation of a superconducting qubit readout and identified important discrepancies between the JC and dispersive models. We expect even larger nondispersive effects when taking into account the multilevel character of low anharmonic qubits such as transmons [35]. This is because the effective dispersive shift is reduced [59], and one requires lower detunings and stronger cavity drives to reach an optimal readout. While the tomography will not change, an optimized simulation of QND readout for multilevel qubits is numerically more challenging [59] and lies outside the scope of this work.

Experimentally, the presented tomography requires only standard control and measurement tools, and therefore it can be immediately implemented to systematically analyze relevant effects on a qubit readout such as the strong driving regime [35,78], leakage to higher levels [79,80], or crosstalk [81,82]. This understanding may help improve the QND measurement performance and guide the design of alternative schemes [36–44]. Moreover, the method can be directly applied to other platforms such as QND detectors of microwave [83–88] or optical photons [89–92]. State preparation and gate errors occurring in experiments can be self-consistently included in the protocol by incorporating standard gate set tomography [72–74]. Furthermore, the reconstruction of high-dimensional Choi matrices could be done more efficiently using compressed sensing [93–96], matrix-product states [97,98], or other advanced techniques [99–105].

From a fundamental point of view, our technique introduces an accurate procedure to quantify the backaction and real QND nature of a measurement via the destructiveness D. This complements the standard analysis in terms of readout fidelity and QND-ness, and allows us to identify regimes of minimal backaction regardless the ideality of the measurement. Nonideal but highly QND measurements may be also exploited for quantum information tasks that require precise evaluations of expectation values [82] since the measurement outcomes can be corrected via error mitigation strategies [55,106,107].

This work has been supported by funding from Spanish Project No. PGC2018-094792-B-I00 (MCIU/AEI/FEDER, UE), CAM/FEDER Project No. S2018/TCS-4342 (QUITEMAD-CM), and CSIC Research Platform on Quantum Technologies PTI-001. L. P. was supported by ANID-PFCHA/DOCTORADO-BECAS-CHILE/2019-772200275. T. R. further acknowledges support from the EU Horizon 2020 program under the Marie Skłodowska-Curie Grant Agreement No. 798397, and from the Juan de la Cierva fellowship IJC2019-040260-I.

*luciano.ivan@iff.csic.es
†t.ramos.delrio@gmail.com

[1] V. B. Braginsky and F. Y. Khalili, *Quantum Measurement* (Cambridge University Press, Cambridge, England, 1992).
[2] H.-P. Breuer and F. Petruccione, *The Theory of Open Quantum Systems* (Oxford University Press, New York, 2002).
[3] G. Colangelo, F. M. Ciurana, L. C. Bianchet, R. J. Sewell, and M. W. Mitchell, Nature (London) **543**, 525 (2017).
[4] C. B. Møller, R. A. Thomas, G. Vasilakis, E. Zeuthen, Y. Tsaturyan, M. Balabas, K. Jensen, A. Schliesser, K. Hammerer, and E. S. Polzik, Nature (London) **547**, 191 (2017).
[5] S. L. Danilishin and F. Y. Khalili, Living Rev. Relativity **15**, 5 (2012).
[6] H. J. Kimble, Y. Levin, A. B. Matsko, K. S. Thorne, and S. P. Vyatchanin, Phys. Rev. D **65**, 022002 (2001).
[7] M. A. C. Rossi, F. Albarelli, D. Tamascelli, and M. G. Genoni, Phys. Rev. Lett. **125**, 200505 (2020).
[8] E. T. Campbell, B. M. Terhal, and C. Vuillot, Nature (London) **549**, 172 (2017).
[9] A. G. Fowler, M. Mariantoni, J. M. Martinis, and A. N. Cleland, Phys. Rev. A **86**, 032324 (2012).
[10] A. Bermudez, X. Xu, M. Gutiérrez, S. C. Benjamin, and M. Müller, Phys. Rev. A **100**, 062307 (2019).
[11] C. Chamberland, K. Noh, P. Arrangoiz-Arriola, E. T. Campbell, C. T. Hann, J. Iverson, H. Putterman, T. C. Bohdanowicz, S. T. Flammia, A. Keller, G. Refael, J. Preskill, L. Jiang, A. H. Safavi-Naeini, O. Painter, and F. G. S. L. Brandão, PRX Quantum **3**, 010329 (2022).
[12] Z. Chen *et al.* (Google Quantum AI Collaboration), arXiv:2102.06132.
[13] D. Leibfried, R. Blatt, C. Monroe, and D. Wineland, Rev. Mod. Phys. **75**, 281 (2003).
[14] M. Raha, S. Chen, C. M. Phenicie, S. Ourari, A. M. Dibos, and J. D. Thompson, Nat. Commun. **11**, 1605 (2020).
[15] J. Volz, R. Gehr, G. Dubois, J. Estève, and J. Reichel, Nature (London) **475**, 210 (2011).
[16] S. Gleyzes, S. Kuhr, C. Guerlin, J. Bernu, S. Deléglise, U. Busk Hoff, M. Brune, J.-M. Raimond, and S. Haroche, Nature (London) **446**, 297 (2007).
[17] P. Grangier, J. A. Levenson, and J.-P. Poizat, Nature (London) **396**, 537 (1998).
[18] P. Neumann, J. Beck, M. Steiner, F. Rempp, H. Fedder, P. R. Hemmer, J. Wrachtrup, and F. Jelezko, Science **329**, 542 (2010).
[19] L. Robledo, L. Childress, H. Bernien, B. Hensen, P. F. A. Alkemade, and R. Hanson, Nature (London) **477**, 574 (2011).
[20] T. Nakajima, A. Noiri, J. Yoneda, M. R. Delbecq, P. Stano, T. Otsuka, K. Takeda, S. Amaha, G. Allison, K. Kawasaki,

A. Ludwig, A. D. Wieck, D. Loss, and S. Tarucha, Nat. Nanotechnol. **14**, 555 (2019).
[21] X. Xue, B. D'Anjou, T. F. Watson, D. R. Ward, D. E. Savage, M. G. Lagally, M. Friesen, S. N. Coppersmith, M. A. Eriksson, W. A. Coish, and L. M. K. Vandersypen, Phys. Rev. X **10**, 021006 (2020).
[22] A. Wallraff, D. I. Schuster, A. Blais, L. Frunzio, J. Majer, M. H. Devoret, S. M. Girvin, and R. J. Schoelkopf, Phys. Rev. Lett. **95**, 060501 (2005).
[23] T. Walter, P. Kurpiers, S. Gasparinetti, P. Magnard, A. Potočnik, Y. Salathé, M. Pechal, M. Mondal, M. Oppliger, C. Eichler, and A. Wallraff, Phys. Rev. Applied **7**, 054020 (2017).
[24] A. Blais, A. L. Grimsmo, S. M. Girvin, and A. Wallraff, Rev. Mod. Phys. **93**, 025005 (2021).
[25] R. Vijay, D. H. Slichter, and I. Siddiqi, Phys. Rev. Lett. **106**, 110502 (2011).
[26] T. Walter, P. Kurpiers, S. Gasparinetti, P. Magnard, A. Potočnik, Y. Salathé, M. Pechal, M. Mondal, M. Oppliger, C. Eichler, and A. Wallraff, Phys. Rev. Applied **7**, 054020 (2017).
[27] M. D. Reed, B. R. Johnson, A. A. Houck, L. DiCarlo, J. M. Chow, D. I. Schuster, L. Frunzio, and R. J. Schoelkopf, Appl. Phys. Lett. **96**, 203110 (2010).
[28] E. Jeffrey, D. Sank, J. Y. Mutus, T. C. White, J. Kelly, R. Barends, Y. Chen, Z. Chen, B. Chiaro, A. Dunsworth, A. Megrant, P. J. J. O'Malley, C. Neill, P. Roushan, A. Vainsencher, J. Wenner, A. N. Cleland, and J. M. Martinis, Phys. Rev. Lett. **112**, 190504 (2014).
[29] E. A. Sete, J. M. Martinis, and A. N. Korotkov, Phys. Rev. A **92**, 012325 (2015).
[30] J. Heinsoo, C. K. Andersen, A. Remm, S. Krinner, T. Walter, Y. Salathé, S. Gasparinetti, J.-C. Besse, A. Potočnik, A. Wallraff, and C. Eichler, Phys. Rev. Applied **10**, 034040 (2018).
[31] D. T. McClure, H. Paik, L. S. Bishop, M. Steffen, J. M. Chow, and J. M. Gambetta, Phys. Rev. Applied **5**, 011001 (R) (2016).
[32] M. Jerger, S. Poletto, P. Macha, U. Hübner, E. Il'ichev, and A. V. Ustinov, Appl. Phys. Lett. **101**, 042604 (2012).
[33] M. Boissonneault, J. M. Gambetta, and A. Blais, Phys. Rev. A **79**, 013819 (2009).
[34] D. H. Slichter, R. Vijay, S. J. Weber, S. Boutin, M. Boissonneault, J. M. Gambetta, A. Blais, and I. Siddiqi, Phys. Rev. Lett. **109**, 153601 (2012).
[35] D. Sank *et al.*, Phys. Rev. Lett. **117**, 190503 (2016).
[36] A. Opremcak, I. V. Pechenezhskiy, C. Howington, B. G. Christensen, M. A. Beck, E. Leonard, J. Suttle, C. Wilen, K. N. Nesterov, G. J. Ribeill, T. Thorbeck, F. Schlenker, M. G. Vavilov, B. L. T. Plourde, and R. McDermott, Science **361**, 1239 (2018).
[37] L. C. G. Govia, E. J. Pritchett, C. Xu, B. L. T. Plourde, M. G. Vavilov, F. K. Wilhelm, and R. McDermott, Phys. Rev. A **90**, 062307 (2014).
[38] I. Siddiqi, R. Vijay, M. Metcalfe, E. Boaknin, L. Frunzio, R. J. Schoelkopf, and M. H. Devoret, Phys. Rev. B **73**, 054510 (2006).
[39] P. Krantz, A. Bengtsson, M. Simoen, S. Gustavsson, V. Shumeiko, W. D. Oliver, C. M. Wilson, P. Delsing, and J. Bylander, Nat. Commun. **7**, 11417 (2016).
[40] R. Dassonneville, T. Ramos, V. Milchakov, L. Planat, E. Dumur, F. Foroughi, J. Puertas, S. Leger, K. Bharadwaj, J. Delaforce, C. Naud, W. Hasch-Guichard, J. J. García-Ripoll, N. Roch, and O. Buisson, Phys. Rev. X **10**, 011045 (2020).
[41] X. Wang, A. Miranowicz, and F. Nori, Phys. Rev. Applied **12**, 064037 (2019).
[42] N. Didier, J. Bourassa, and A. Blais, Phys. Rev. Lett. **115**, 203601 (2015).
[43] S. Touzard, A. Kou, N. E. Frattini, V. V. Sivak, S. Puri, A. Grimm, L. Frunzio, S. Shankar, and M. H. Devoret, Phys. Rev. Lett. **122**, 080502 (2019).
[44] T. Noh, Z. Xiao, K. Cicak, X. Y. Jin, E. Doucet, J. Teufel, J. Aumentado, L. C. G. Govia, L. Ranzani, A. Kamal, and R. W. Simmonds, arXiv:2103.09277.
[45] J. S. Lundeen, A. Feito, H. Coldenstrodt-Ronge, K. L. Pregnell, C. Silberhorn, T. C. Ralph, J. Eisert, M. B. Plenio, and I. A. Walmsley, Nat. Phys. **5**, 27 (2009).
[46] A. Luis and L. L. Sánchez-Soto, Phys. Rev. Lett. **83**, 3573 (1999).
[47] G. M. D'Ariano, L. Maccone, and P. Lo Presti, Phys. Rev. Lett. **93**, 250407 (2004).
[48] J. Fiurášek, Phys. Rev. A **64**, 024102 (2001).
[49] Y. Chen, M. Farahzad, S. Yoo, and T.-C. Wei, Phys. Rev. A **100**, 052315 (2019).
[50] K. Rudinger, G. J. Ribeill, L. C. G. Govia, M. Ware, E. Nielsen, K. Young, T. A. Ohki, R. Blume-Kohout, and T. Proctor, arXiv:2103.03008.
[51] J. Z. Blumoff, K. Chou, C. Shen, M. Reagor, C. Axline, R. T. Brierley, M. P. Silveri, C. Wang, B. Vlastakis, S. E. Nigg, L. Frunzio, M. H. Devoret, L. Jiang, S. M. Girvin, and R. J. Schoelkopf, Phys. Rev. X **6**, 031041 (2016).
[52] In this work, the Choi matrix Υ_n^{ijkl} encodes the transformation of the density matrix [53], while $\tilde{\Upsilon}_n^{ijkl} = \Upsilon_n^{ikjl}$ is a transposed version that is Hermitian and non-negative.
[53] S. Milz, F. A. Pollock, and K. Modi, Open Syst. Inf. Dyn. **24**, 1740016 (2017).
[54] A. Vourdas, Opt. Commun. **76**, 164 (1990).
[55] M. Ban, Phys. Lett. A **249**, 167 (1998).
[56] D. F. V. James, P. G. Kwiat, W. J. Munro, and A. G. White, Phys. Rev. A **64**, 052312 (2001).
[57] J. Shang, Z. Zhang, and H. K. Ng, Phys. Rev. A **95**, 062336 (2017).
[58] We solve each minimization problem using sequential least squares programming, satisfying the positivity of operators via the Cholesky decomposition, and the completeness constraints via Lagrange multipliers.
[59] See Supplemental Material at http://link.aps.org/supplemental/10.1103/PhysRevLett.129.010402 for details on (i) the calculation of destructiveness and applications of nonideal QND measurements, (ii) the simulation of qubit readout with the stochastic master equation, (iii) the explicit form of Choi matrices in the dispersive model, (iv) the effect of qubit decoherence on Choi matrices, (v) the effect of outcome discrimination criteria on Choi matrices, and (vi) a discussion on the multilevel character of qubits in QND readout.

[60] A. Peruzzo, J. McClean, P. Shadbolt, M.-H. Yung, X.-Q. Zhou, P. J. Love, A. Aspuru-Guzik, and J. L. O'Brien, Nat. Commun. **5**, 4213 (2014).

[61] A. Kandala, A. Mezzacapo, K. Temme, M. Takita, M. Brink, J. M. Chow, and J. M. Gambetta, Nature (London) **549**, 242 (2017).

[62] V. Havlíček, A. D. Córcoles, K. Temme, A. W. Harrow, A. Kandala, J. M. Chow, and J. M. Gambetta, Nature (London) **567**, 209 (2019).

[63] R. T. Thew, K. Nemoto, A. G. White, and W. J. Munro, Phys. Rev. A **66**, 012303 (2002).

[64] C. L. Degen, F. Reinhard, and P. Cappellaro, Rev. Mod. Phys. **89**, 035002 (2017).

[65] A. Blais, R. S. Huang, A. Wallraff, S. M. Girvin, and R. J. Schoelkopf, Phys. Rev. A **69**, 062320 (2004).

[66] L. C. G. Govia and F. K. Wilhelm, Phys. Rev. A **93**, 012316 (2016).

[67] H. M. Wiseman and G. J. Milburn, *Quantum Measurement and Control* (Cambridge University Press, Cambridge, England, 2010).

[68] J. Gambetta, A. Blais, M. Boissonneault, A. A. Houck, D. I. Schuster, and S. M. Girvin, Phys. Rev. A **77**, 012112 (2008).

[69] C. Laflamme, D. Yang, and P. Zoller, Phys. Rev. A **95**, 043843 (2017).

[70] D. Yang, C. Laflamme, D. V. Vasilyev, M. A. Baranov, and P. Zoller, Phys. Rev. Lett. **120**, 133601 (2018).

[71] K. Jacobs, *Stochastic Processes for Physicists: Understanding Noisy Systems* (Cambridge University Press, Cambridge, England, 2010).

[72] S. T. Merkel, J. M. Gambetta, J. A. Smolin, S. Poletto, A. D. Córcoles, B. R. Johnson, C. A. Ryan, and M. Steffen, Phys. Rev. A **87**, 062119 (2013).

[73] D. Greenbaum, arXiv:1509.02921.

[74] J. P. Dehollain, J. T. Muhonen, R. Blume-Kohout, K. M. Rudinger, J. K. Gamble, E. Nielsen, A. Laucht, S. Simmons, R. Kalra, A. S. Dzurak, and A. Morello, New J. Phys. **18**, 103018 (2016).

[75] T. Yamamoto, K. Inomata, K. Koshino, P.-M. Billangeon, Y. Nakamura, and J. S. Tsai, New J. Phys. **16**, 015017 (2014).

[76] F. Yan, S. Gustavsson, A. Kamal, J. Birenbaum, A. P. Sears, D. Hover, T. J. Gudmundsen, D. Rosenberg, G. Samach, S. Weber, J. L. Yoder, T. P. Orlando, J. Clarke, A. J. Kerman, and W. D. Oliver, Nat. Commun. **7**, 12964 (2016).

[77] Refining the discrimination criteria between measurement outcomes does not change this behavior [59].

[78] M. Boissonneault, J. M. Gambetta, and A. Blais, Phys. Rev. Lett. **105**, 100504 (2010).

[79] F. Motzoi, J. M. Gambetta, P. Rebentrost, and F. K. Wilhelm, Phys. Rev. Lett. **103**, 110501 (2009).

[80] C. Wang, M.-C. Chen, C.-Y. Lu, and J.-W. Pan, Fundam. Res. **1**, 16 (2021).

[81] K. E. Hamilton, T. Kharazi, T. Morris, A. J. McCaskey, R. S. Bennink, and R. C. Pooser, arXiv:2006.01805.

[82] S. Bravyi, S. Sheldon, A. Kandala, D. C. Mckay, and J. M. Gambetta, Phys. Rev. A **103**, 042605 (2021).

[83] S. Kono, K. Koshino, Y. Tabuchi, A. Noguchi, and Y. Nakamura, Nat. Phys. **14**, 546 (2018).

[84] J.-C. Besse, S. Gasparinetti, M. C. Collodo, T. Walter, P. Kurpiers, M. Pechal, C. Eichler, and A. Wallraff, Phys. Rev. X **8**, 021003 (2018).

[85] R. Lescanne, S. Deléglise, E. Albertinale, U. Réglade, T. Capelle, E. Ivanov, T. Jacqmin, Z. Leghtas, and E. Flurin, Phys. Rev. X **10**, 021038 (2020).

[86] R. Dassonneville, R. Assouly, T. Peronnin, P. Rouchon, and B. Huard, Phys. Rev. Applied **14**, 044022 (2020).

[87] A. Essig, Q. Ficheux, T. Peronnin, N. Cottet, R. Lescanne, A. Sarlette, P. Rouchon, Z. Leghtas, and B. Huard, Phys. Rev. X **11**, 031045 (2021).

[88] J. C. Curtis, C. T. Hann, S. S. Elder, C. S. Wang, L. Frunzio, L. Jiang, and R. J. Schoelkopf, Phys. Rev. A **103**, 023705 (2021).

[89] A. I. Lvovsky and M. G. Raymer, Rev. Mod. Phys. **81**, 299 (2009).

[90] M. Lobino, D. Korystov, C. Kupchak, E. Figueroa, B. C. Sanders, and A. I. Lvovsky, Science **322**, 563 (2008).

[91] L. Zhang, H. B. Coldenstrodt-Ronge, A. Datta, G. Puentes, J. S. Lundeen, X.-M. Jin, B. J. Smith, M. B. Plenio, and I. A. Walmsley, Nat. Photonics **6**, 364 (2012).

[92] T. Ramos and J. J. García-Ripoll, Phys. Rev. Lett. **119**, 153601 (2017).

[93] D. Gross, Y.-K. Liu, S. T. Flammia, S. Becker, and J. Eisert, Phys. Rev. Lett. **105**, 150401 (2010).

[94] C. A. Riofrío, D. Gross, S. T. Flammia, T. Monz, D. Nigg, R. Blatt, and J. Eisert, Nat. Commun. **8**, 15305 (2017).

[95] D. Ahn, Y. S. Teo, H. Jeong, F. Bouchard, F. Hufnagel, E. Karimi, D. Koutný, J. Řeháček, Z. Hradil, G. Leuchs, and L. L. Sánchez-Soto, Phys. Rev. Lett. **122**, 100404 (2019).

[96] D. Ahn, Y. S. Teo, H. Jeong, D. Koutný, J. Řeháček, Z. Hradil, G. Leuchs, and L. L. Sánchez-Soto, Phys. Rev. A **100**, 012346 (2019).

[97] M. Cramer, M. B. Plenio, S. T. Flammia, R. Somma, D. Gross, S. D. Bartlett, O. Landon-Cardinal, D. Poulin, and Y.-K. Liu, Nat. Commun. **1**, 149 (2010).

[98] B. P. Lanyon, C. Maier, M. Holzäpfel, T. Baumgratz, C. Hempel, P. Jurcevic, I. Dhand, A. S. Buyskikh, A. J. Daley, M. Cramer, M. B. Plenio, R. Blatt, and C. F. Roos, Nat. Phys. **13**, 1158 (2017).

[99] G. Tóth, W. Wieczorek, D. Gross, R. Krischek, C. Schwemmer, and H. Weinfurter, Phys. Rev. Lett. **105**, 250403 (2010).

[100] D. Goyeneche, G. Cañas, S. Etcheverry, E. S. Gómez, G. B. Xavier, G. Lima, and A. Delgado, Phys. Rev. Lett. **115**, 090401 (2015).

[101] L. Zambrano, L. Pereira, and A. Delgado, Phys. Rev. A **100**, 022340 (2019).

[102] C. Carmeli, T. Heinosaari, M. Kech, J. Schultz, and A. Toigo, Europhys. Lett. **115**, 30001 (2016).

[103] L. Zambrano, L. Pereira, D. Martínez, G. Cañas, G. Lima, and A. Delgado, Phys. Rev. Applied **14**, 064004 (2020).

[104] L. Pereira, L. Zambrano, and A. Delgado, npj Quantum Inf. **8**, 57 (2022).

[105] A. Farooq, J. ur Rehman, and H. Shin, arXiv:2111.11071.

[106] L. Botelho, A. Glos, A. Kundu, J. A. Miszczak, O. Salehi, and Z. Zimborás, Phys. Rev. A **105**, 022441 (2022).

[107] M. R. Geller, Phys. Rev. Lett. **127**, 090502 (2021).